Nickel N-heterocyclic carbene complexes in homogeneous catalysis

Berding, J.

Chapter 6

Theoretical study on the Kumada coupling catalyzed by bisNHC nickel complexes[†]

Abstract. *The complete catalytic cycle of the Kumada coupling of aryl halides with aryl Grignard reagents using a nickel complex with a chelating bis(N-heterocyclic carbene) ligand has been calculated using density functional theory. The results indicate that the three steps of the catalytic cycle have barriers of similar magnitude, in agreement with the experimentally observed change in the rate-limiting step with a change of the leaving group. Moreover, the route towards the various experimentally-observed side products was calculated to originate from an aryl-exchange pathway that arises during the transmetalation step.*

[†] Based on: J. Berding, F. Buda, A. W. Ehlers, E. Bouwman, *J. Organomet. Chem.*, *in preparation*.

6.1 Introduction

Transition-metal catalyzed cross-coupling reactions, such as the Suzuki and Stille reactions have become important tools in modern organic synthesis.[1, 2] A substantial number of papers has been focused on the elucidation of the mechanism of these cross-coupling reactions, often aided by calculations based on density functional theory (DFT). Most of these investigations are dealing with palladium catalysts bearing phosphane ligands. Especially the oxidative addition of aryl halides to Pd(0) complexes received much attention.[3-6]

Even though the Kumada coupling was discovered more than 35 years ago,[7, 8] only few attempts have been made to investigate its proposed mechanism (Scheme 6.1)[9] using theoretical calculations. The main reason for this appears to be the fact that soon after the Kumada coupling was discovered many other types of catalytic aryl-aryl couplings were found. These other reactions proved to be more versatile, had better functional group tolerance, and have been studied in more detail. Still, often their starting compounds are less reactive and have to be prepared from a Grignard reagent. The advantage of the Kumada coupling is therefore that it eliminates one synthetic step, as it uses the Grignard reagent in the catalytic reaction.

The work on the nickel-catalyzed Kumada coupling of aryl halides with aryl Grignard reagents is described in Chapter 4.[10] The catalysts used in that study are based on nickel(II) dihalide complexes, bearing bidentate bis(N-heterocyclic carbene) (bisNHC) ligands (Figure 6.1, **I**),[10] which were used to catalytically couple 4-haloanisoles (**i_X**, X = Cl, Br) with phenylmagnesium chloride (**ii**) (Scheme 6.2). This yielded 4-methoxybiphenyl (**iii**) in varying yields and at varying rates, depending on the leaving group of the reagent (**i_X**) and the side groups and bridging moiety of the ligand of the nickel catalyst. In addition, a number of side products could be identified, *i. e.* biphenyl (**iv**), anisole (**v**), and 4,4-dimethoxy-biphenyl (**vi**).

It was observed that the rate of the reaction strongly depends on the bulk of the ligand used. The coupling of 4-chloroanisole proceeds at a higher rate when larger side-groups are present on the ligand, while starting from 4-bromoanisole the

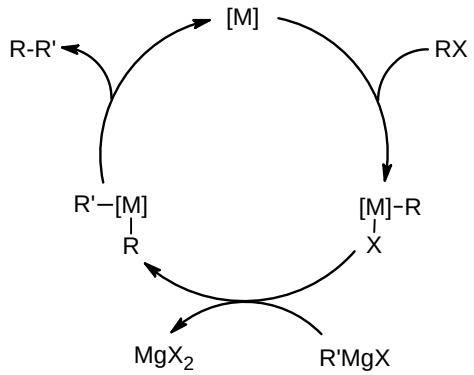

Scheme 6.1. Proposed catalytic cycle of the Kumada coupling (adapted from ref. 9).

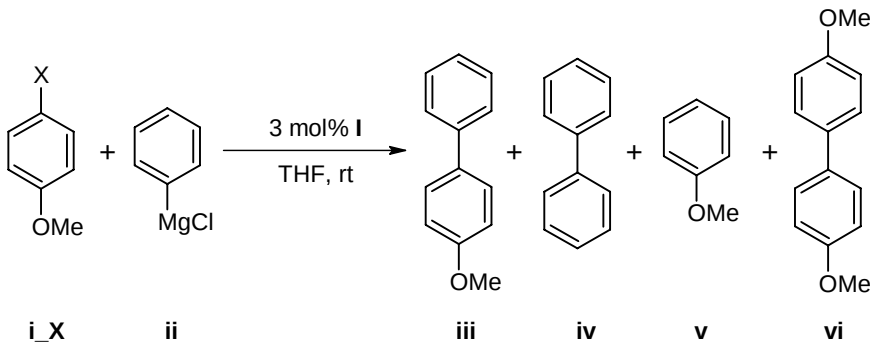

Scheme 6.2. Products of the nickel-catalyzed Kumada coupling as experimentally observed.

opposite is observed. This difference was tentatively ascribed to a change in the rate-determining step; for the chloride-containing reagent the reductive elimination is most likely to be rate-determining, while for the bromide-containing reagent it should be either the oxidative addition or the transmetalation step.[10]

To the best of our knowledge, so far no attempts have been made to calculate the complete catalytic cycle of the Kumada coupling by quantum mechanical calculations. Only recently, Yoshikai *et al.* reported their studies of the Kumada coupling of 2-halotoluene catalyzed by a nickel diphosphane complex, making use of an analysis of kinetic isotope effects (KIEs) and DFT calculations.[11]

N-Heterocyclic carbene complexes have been investigated by quantum-mechanical computational tools a number of times. For instance, the nature of the NHC-metal bond has been studied in detail,[12, 13] and some reports deal with NHC ligands in catalysis.[14]

In this chapter, the results of quantum-chemical calculations of the complete catalytic cycle of the Kumada coupling (Scheme 6.1) with a nickel bisNHC complex are reported, and the data are used to rationalize the trends observed in catalytic experiments.[10] In addition, a possible route has been calculated that may explain the formation of the various side products that are observed experimentally.

6.2 Computational Details

All calculations were performed using the Amsterdam Density Functional (ADF) 2006.01 program packages.[15-17] The density functional calculations (DFT) with the BLYP functional[18, 19] employed a basis set of triple-ζ quality, which is denoted TZP in ADF. Geometries were fully optimized, normally without symmetry constraints. Analytical frequency calculations were performed at the same level of theory and used to identify stationary points (no imaginary frequencies) and transition states (one large imaginary frequency, corresponding to the nuclear motion along the reaction coordinate under study). Furthermore, the frequency calculations were used to determine zero-point energy (ZPE) corrected bonding energies and the Gibbs free energy at 298 K.

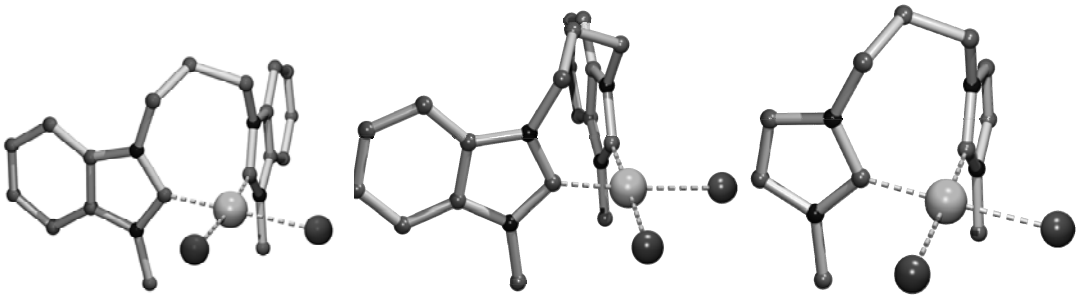

Figure 6.1. Geometry comparison of the solid state structure of full complex **I** (R = Me, R' = 1,3-propanediyl), calculated full complex **I** and the calculated structure of the smaller system **II** at the BLYP/TZP level of theory used in this chapter.

Solvent effects were taken into account for all of the systems under study through single-point calculations at each optimized geometry using the conductor-like screening model (COSMO)[20, 21]. In this model the molecule under investigation is placed in a cavity, which has the shape of this molecule.[22] Outside this cavity, the solvent is calculated as a homogeneous dielectric medium, which is polarized by the charge distribution. The response of the medium is described by the generation of screening charges on the cavity surface. The electrostatic interaction between the molecule and the solvent is calculated through the solvent-induced cavity surface charges. In this study the solvent (tetrahydrofuran) had the following parameters: dielectric constant = 7.58, radius = 3.18 Å.

6.3 Results and Discussion

6.3.1 Model and test calculations

To limit the computational workload, a slightly modified, simplified system was used in the DFT calculations. The bisNHC ligand was reduced in size by replacing the benzimidazole moieties by imidazoles (Figure 6.1, **II**). Even though the free imidazol-2-ylidene and benzimidazol-2-ylidenes are known to behave differently in solution,[23] their properties as ligands are expected to be comparable. As bridging moiety the $(CH_2)_3$-chain was selected, which was calculated completely, as it exerts strain on the *cis* chelating ligand. The methyl substituents were maintained for steric and electronic reasons, even though some reports use H-substituted NHCs in calculations.[13] The methoxy group of the 4-haloanisole reagent used in the catalytic reaction was not included in the calculations, as it was included in catalysis mainly to discriminate between product and side products and is not considered to be essential for the reaction. Furthermore, the influence of the methoxy group on the oxidative addition to a palladium phosphane complex was calculated to be small in comparison to a system without this substituent.[3]

To justify executing calculations at the BLYP/TZP level of theory and the use of the smaller imidazole-based ligand instead of the full benzimidazole moiety, the structure of the full starting complex **I** (R = Me, R' = 1,3-propanediyl) and the smaller complex $LNiBr_2$ (**II**), (L is 1,1'-dimethyl-3,3'-(1,3-propanediyl)-bisimidazol-2,2'-diylidene), were calculated and compared to the known solid-state structure of **I** (Figure 6.1).[10] Selected structural parameters are listed in Table 6.1. The calculated parameters for complex **I** correspond well to the experimental data. The Ni–Br distance is slightly overestimated, as is the C–C bite angle; however, as packing effects are not included in the calculations and as these calculations place the structures in a vacuum, some deviations are to be expected. The bond distances and angles calculated for the trimmed-down complex **II** are in line with those found for the larger complex **I**. As expected, the C–C backbone of the imidazole ring is shorter, as it is now a double bond and not part of an aromatic benzene ring. The absence of the aromatic rings in complex **II** causes a slight lengthening of the Ni–C bond from 1.88 to 1.90 Å.

Because of the high bond-dissociation energy of metal-carbene bonds observed experimentally,[24] the possibility of dissociation of the NHC ligand was not taken into consideration and indeed during the calculations lengthening of the Ni–C_{NHC} bond indicating dissociation was not observed. Furthermore, the possibility of *cis*/*trans* isomerization of the bidentate ligand was not taken into account. For monodentate ligands this is expected to occur during the catalytic cycle, however, due to the bridging moiety the ligand C donors should remain in *cis* positions.

In addition to the gas-phase calculations, the conductor-like screening model (COSMO) was used to estimate the implicit effect of the solvent (THF) on the

Table 6.1. Selected bond lengths (Å) and angles (°) of the solid–state structure of compound **I** (R = Me, R' = 1,3-propanediyl), calculated compound **I**, and calculated compound **II** (X = Br).

	$\mathbf{I}_{Exp.}$ (avgd.)	$\mathbf{I}_{Calc.}$ (avgd.)	$\mathbf{II}_{Calc.}$
Ni–Br	2.36	2.43	2.43
Ni–C	1.86	1.88	1.90
C-C backbone	1.38	1.41	1.36
Br1–Ni–Br2	96.0	96.5	95.4
C12–Ni–C22	85.8	90.8	91.4
NCN	106.8	106.1	104.5
NiC_2 / carbene dihedral angle[a]	84.0	80.1	78.1

[a] NiC_2 / Carbene dihedral angle = angle between LS planes; one through the imidazole ring; one through the NiC_2-coordination plane.

Table 6.2. Energies (kcal mol^{-1}) related to the coordination of THF to magnesium compounds.

[Mg] + n THF → [Mg](THF)$_n$

	ΔE_{ZPE}			ΔG_{gas}			ΔG_{THF}		
n	$MgCl_2$	MgBrCl	PhMgCl	$MgCl_2$	MgBrCl	PhMgCl	$MgCl_2$	MgBrCl	PhMgCl
1	–21.2	–23.6	–17.2	–9.5	–10.0	–6.2	–5.9	–7.1	–2.6
2	–39.0	–41.2	–30.7	–16.6	–16.9	–7.2	–9.7	–10.7	–1.1
3	–42.1	–43.9		–5.8	–7.1		5.2	3.0	
4[a]	–45.4	–47.1		2.8	3.1		16.6	15.6	

[a] Only the *trans* complex was calculated

reaction free energy of all structures. Explicit solvent interactions were taken into account for two coordinatively unsaturated metal centers. The coordination of THF to coordinatively unsaturated Ni(0) complex **1** (see below) was calculated to be slightly endothermic and entropically unfavorable (ΔE_{ZPE} = 3.7 kcal mol^{-1} , ΔG_{THF} = 18.8 kcal mol^{-1}). The interaction of THF and other ethers with Grignard reagents and other magnesium salts has been investigated experimentally,[25, 26] and computationally[27, 28] several times. Even though these reports are not always in agreement, it is clear that solvent interaction is important. Therefore, it was decided to calculate the structures and energies of all magnesium starting materials and products with explicit THF coordination.

The energies (Table 6.2) related to the coordination of varying equivalents of THF to $MgCl_2$, MgBrCl and phenylmagnesium chloride, and the structures (the chloride compounds are depicted in Figure 6.2) of the adducts MgXCl(THF)$_n$ (n = 1 – 4) and PhMgCl(THF)$_n$ (n = 1, 2) were calculated at the BLYP/TZP level of theory. In agreement with previous results,[28] the coordination of two molecules of THF was energetically most favourable for magnesium dihalide salts, when implicit solvent corrections are taken into account (ΔG_{THF} = –9.7 kcal mol^{-1} for $MgCl_2$, –10.7 kcal mol^{-1} for MgBrCl). The present calculations reveal that the most stable THF adduct of phenylmagnesium chloride has only one THF coordinated to it (ΔG_{THF} = –2.6 kcal mol^{-1} for PhMgCl), however, with only a small energy difference, compared to the coordination of two THF molecules.

The overall reaction (1) was calculated to be highly exothermic and exergonic: ΔE_{ZPE} = –73.4 kcal mol^{-1}, ΔG_{THF} = –59.9 for X = Cl and ΔE_{ZPE} = –74.5 kcal mol^{-1}, ΔG_{THF} = –59.6 kcal mol^{-1}, for X = Br.[29]

$$PhX + PhMgCl(THF) + THF \rightarrow PhPh + MgXCl(THF)_2 \qquad (1)$$

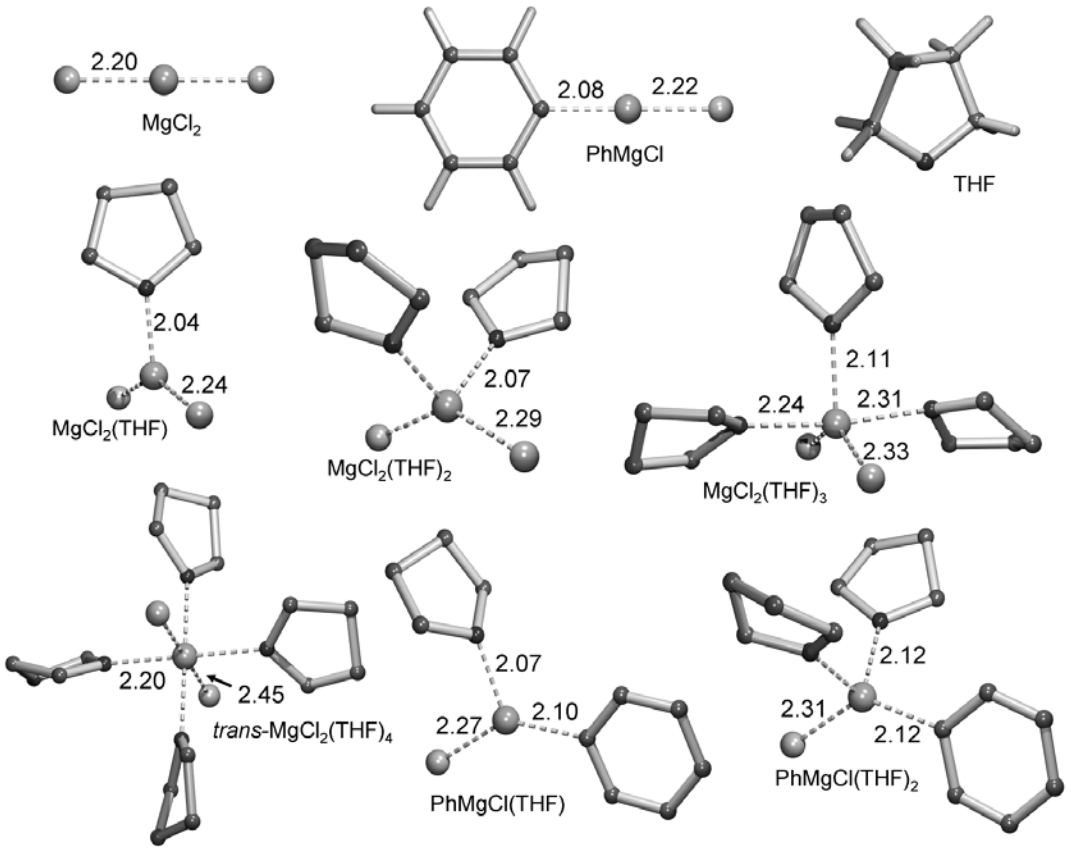

Figure 6.2. Calculated structures of the species involved in the coordination of THF to magnesium compounds. Selected bond lengths are given in Å. Hydrogen atoms are omitted from the THF adducts for clarity.

6.3.2 The catalytic cycle

General

The generally accepted mechanism for the nickel-catalyzed Kumada coupling, schematically shown in Scheme 6.1, consists of three consecutive steps: oxidative addition of the aryl halide, transmetalation of the aryl moiety of the Grignard reagent to the nickel center and finally reductive elimination of the biaryl product. These three steps are discussed separately below. The starting point of the catalytic cycle is a nickel(0) complex. Under experimental conditions this species is obtained from the starting nickel(II) complex **I** by a transmetalation of both halides (see below), followed by reductive elimination of biphenyl.

The relative enthalpies with zero-point energy correction (ΔE_{ZPE}), the gas-phase Gibbs free energies (ΔG_{gas}) and the relative Gibbs free energies with COSMO solvent correction (ΔG_{THF}) for all calculated species are listed in Table 6.3. The following discussion is mainly focused on the solvent-corrected relative Gibbs free energies, ΔG_{THF}.

Table 6.3. Relative total energies (kcal mol^{-1}) with zero-point correction, gas-phase Gibbs free energies and COSMO–THF corrected Gibbs free energies for the species along the oxidative addition, transmetalation, aryl exchange and reductive elimination steps.[a]

	X = Cl			X = Br		
Structure	ΔE_{ZPE}	ΔG_{gas}	ΔG_{THF}	ΔE_{ZPE}	ΔG_{gas}	ΔG_{THF}
1 + PhX	0.0	0.0	0.0	0.0	0.0	0.0
2_X	–10.6	1.7	1.3	–12.9	–0.4	–2.0
TS$_{23}$X	8.3	21.6	24.1	7.4	21.1	24.7
3_X	–38.8	–26.4	–41.1	–42.2	–29.3	–43.1
3_X + PhMgCl(THF) + THF	0.0	0.0	0.0	0.0	0.0	0.0
4_X + 2 THF	–4.8	–3.0	6.3	–2.2	1.3	9.5
TS$_{45}$X + 2 THF	5.3	10.7	20.9	7.5	12.0	21.2
5_X + 2 THF	–8.6	–2.1	4.5	–6.2	–0.2	7.1
6 + MgXCl(THF)$_2$	–31.2	–16.9	–9.8	–28.8	–14.9	–7.5
6	0.0	0.0	0.0			
TS$_{67}$	14.7	16.1	20.9			
7	–2.3	–0.9	9.8			
8	–11.4	–11.4	–1.9			
1 + PhPh	–3.5	–15.3	–9.0			

[a] For every step the energies are reported relative to the first species of that step.

Oxidative addition

Theoretical investigations into the insertion of zerovalent group-10 transition metals, most notably palladium, into carbon-halide bonds has been the subject of a number of recent papers.[3-6] The reason for this interest is that this process is often the rate-determining step in a catalytic cycle. In a number of papers the oxidative addition is proposed to take place starting from an η^2-coordinated aryl halide.[30, 31] In addition, evidence is available that the metal may coordinate to different C–C bonds in sequence before the actual oxidative addition takes place, *i.e.* in a ring-walking

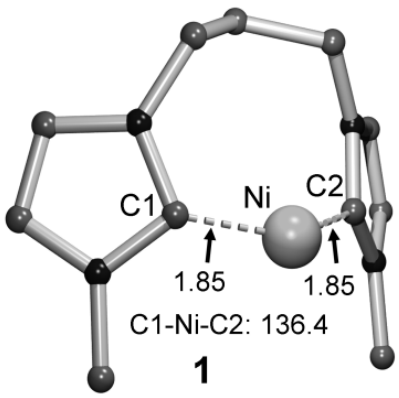

Figure 6.3. Geometry of starting nickel(0) species **1** with calculated bond distances (Å) and angles (°). Hydrogen atoms are omitted for clarity.

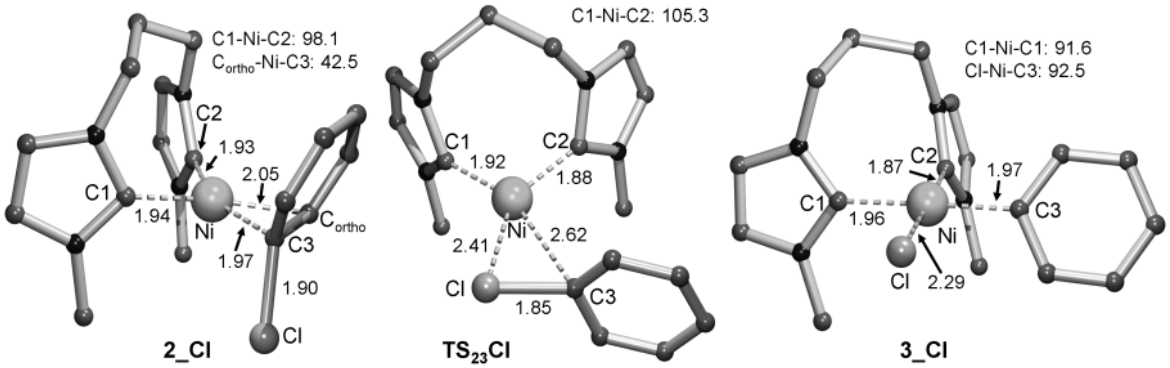

Figure 6.4. Geometries of the species in the oxidative addition step with calculated bond distances (Å) and angles (°) for the chloride compounds. Hydrogen atoms are omitted for clarity.

mechanism. Such ring-walking calculations were not performed for the present system, as the barriers have been calculated to be small for the nickel bisphosphane complex.[11]

The bisNHC ligand in the starting nickel(0) species **1** (Figure 6.3) was calculated to have a bite angle of 136.4°. It is known from experimental data that nickel(0) species bearing two monodentate NHC ligands adopt a linear geometry,[32] however, the propylene bridging group keeps the two carbene rings closer to each other. The Ni–C bonds are relatively short, compared to the nickel(II) species **II** (1.85 and 1.90 Å, respectively), and are comparable to other calculated Ni(0)-NHC distances.[13]

The calculated structures for the oxidative addition sequence with selected structural parameters (for the chloride compounds) are depicted in Figure 6.4 and the relative energies are plotted in Scheme 6.3. The aryl halide coordinates to the nickel(0) species **1** in a η^2 fashion to form the pre-reactive π-complex **2_X**. The Ni–C3

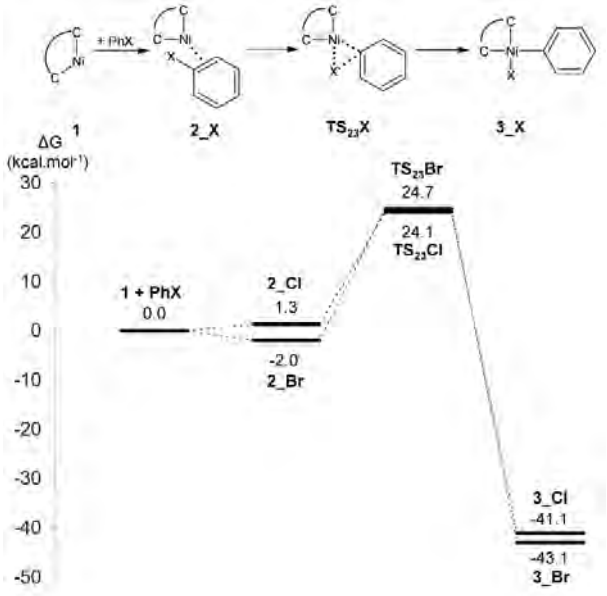

Scheme 6.3. Energy diagram for the oxidative addition step. Energies are given as Gibbs free energy in solution (THF, COSMO) relative to **1** + PhX.

bond is slightly longer than the Ni–C_{ortho} bond, due to the electronegative halide on C3. The bidentate ligand is reoriented, resulting in a trigonal geometry around the nickel center, with a bite-angle of 98.1° and 97.9° for X = Cl and Br, respectively.

The coordination of the aryl halide is favored by total energy (ΔE_{ZPE} = –10.6 and –12.9 kcal mol^{-1} for X = Cl and Br, respectively), but is entropically disfavored, giving a total solvent-corrected free energy of 1.3 and –2.0 kcal mol^{-1} for X = Cl and Br, respectively.

The π-complex is transformed into a three-center transition state **TS_{23}_X**, with an imaginary frequency corresponding to a cleavage of the C3–X bond. This leads to an increase of the free energy of 22.7 and 26.7 kcal mol^{-1} for X = Cl and Br, respectively, and a widening of the bisNHC bite angle to 105.3° and 113.7°. The C3–X bond is slightly shortened, while the Ni–C3 bond is significantly longer than in species **2_X**. The shorter C3–X bond suggests that another intermediate, with coordination of the nickel center to the C3–X bond, should be present; however, attempts to locate this intermediate were unsuccessful.

The transition state leads to a cleavage of the C–X bond yielding the nickel(II) species **3_X**, with the halide and the phenyl ring in *cis* positions. Due to the strong *trans* effect of the phenyl ring, the Ni–C1 bond is significantly longer than the Ni–C2 bond. As the Ni–X and Ni–C3 bonds are now fully formed, they are shorter than those in transition state **TS_{23}X**. Overall, starting from complex **1** and phenyl halide, the oxidative addition is highly exothermic. The total gain in solvent-corrected free energy is 41.1 and 43.1 kcal mol^{-1}, for X = Cl and Br, respectively. The oxidative addition of chlorobenzene to $Ni(PH_3)_2$ was calculated to have a barrier of 8.9 kcal mol^{-1} and a total gain in energy of 19.1 kcal mol^{-1}.[33] The difference between the present NHC system and the phosphane species may be due to the fact that NHCs are more electron donating than phosphanes.

Transmetalation

Even though the transmetalation steps of a number of C–C cross coupling reactions have been investigated theoretically,[34] in the case of the Kumada coupling this step has not received a lot of attention. Generally, a 4-membered cyclic transition state is assumed for the exchange of the halide of the transition metal and the organic moiety on the donating fragment.[35] The intermediates and transition state calculated for the transmetalation steps are shown in Figure 6.5 (for the chloride compounds),[36] the corresponding relative free energies are plotted in Scheme 6.4.

The transmetalation sequence starts with the formation of adduct **4_X** from complex **3_X** and phenylmagnesium chloride, accompanied by a loss of the THF molecule which was coordinated to the latter. The magnesium ion is located between the halide and the aryl ring of the nickel complex thus forming a 4-membered ring, and adopts a distorted tetrahedral geometry. The nickel halide and nickel phenyl

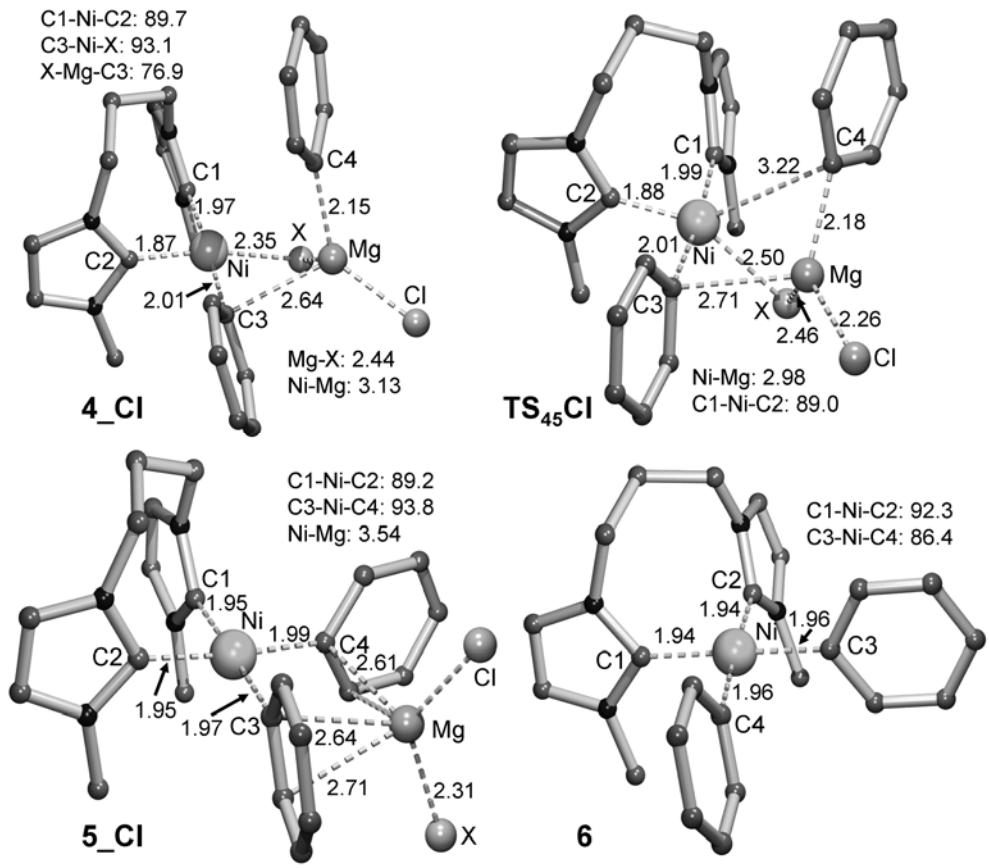

Figure 6.5. Geometries of the species in the transmetalation step (X = Cl) with calculated bond distances (Å) and angles (°). Hydrogen atoms are omitted for clarity.

bonds are slightly elongated. In addition to this geometry, another, less stable structure was calculated in which the magnesium ion is only coordinated to the nickel halide. Possibly, this alternative structure is an intermediate for the formation of **4_X**, however, no transition state between the two could be located. The formation of adduct **4_X** is endothermic, with ΔG_{THF} = 6.3 and 9.5 kcal mol^{-1} for X = Cl and Br, respectively, of which 2.6 kcal mol^{-1} is due to the dissociation of the THF molecule.

The following transition state **TS$_{45}$X**, which has an imaginary vibration equivalent to a rotation around the Mg–C3 bond, brings the magnesium-bound phenyl ring closer to the nickel center, while the halide is moved away from the nickel center. The magnesium ion remains in a tetrahedral geometry, including a weak interaction with the non-reactive nickel-bound phenyl ring. The Ni–C4–Mg–X 4-membered ring is highly distorted, with a short Ni–Mg distance of 2.98 and 3.07 Å, for X = Cl and Br, respectively.

The transition state is 20.9 and 21.2 kcal mol^{-1} for X = Cl and Br, respectively, higher in energy than the starting complex **3_X** and PhMgCl(THF) and leads to intermediate **5_X**, in which an MgXCl moiety is located between the two nickel-bound phenyl rings, with π coordination to both rings. The free energies of **4_X** and **5_X** are of comparable magnitude. The subsequent release of MgXCl from complex **5_X** yields complex **6**; simultaneous coordination of two THF solvent molecules to

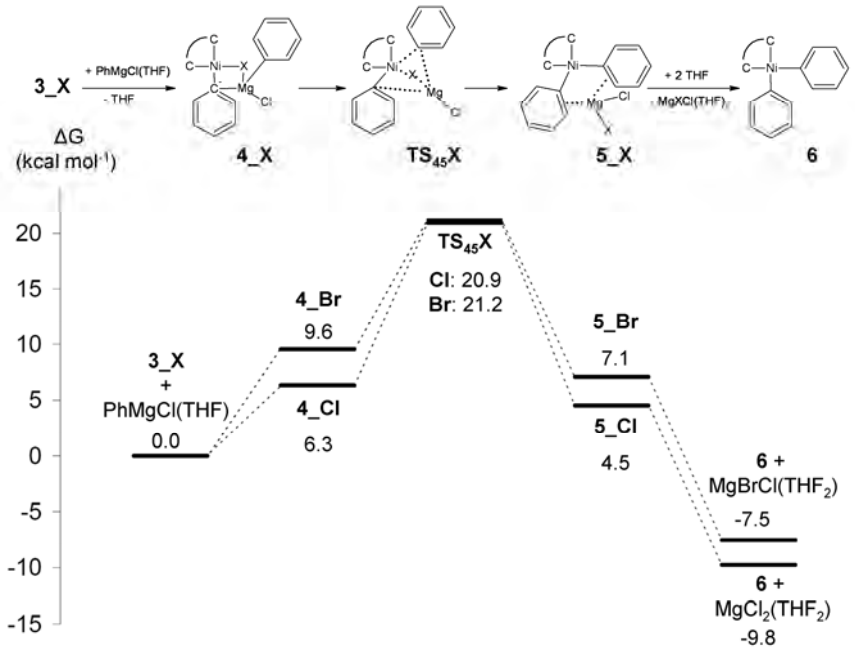

Scheme 6.4. Energy diagram for the transmetalation step. Energy is given as Gibbs free energy in solution (THF, COSMO) relative to **3_X** + PhMgCl(THF) + THF.

MgXCl lowers the free energy by 14.3 and 14.6 kcal mol^{-1}, for X = Cl and Br, respectively, of which 9.7 and 10.7 kcal mol^{-1} is due to the solvent coordination. Species **6** has a slightly distorted square-planar C_4 coordination sphere, with both phenyl rings perpendicular to the coordination plane.

In addition to the structures depicted in Figure 6.5, alternative structures in which the phenylmagnesium chloride is initially coordinated with the phenyl ring and the chloride anion located on exchanged positions on the magnesium ion were considered. However, initial calculations showed only small energy differences compared to those reported above, and these alternative structures not taken into account.

Reductive elimination

The last step in the catalytic cycle is the reductive elimination of the product. In this process the nickel center is formally reduced from the 2+ to the 0 oxidation state, while two Ni–C bonds are broken and a new C–C bond is formed. This step is well known for sp^3 carbons, however, few theoretical studies are available for unsaturated carbon ligands.[37, 38] The species involved in the reductive elimination are depicted in Figure 6.6. The relative energies of these species are plotted in Scheme 6.5.

The two phenyl rings of **6** approach each other to give a new C–C bond, via transition state **TS$_{67}$**. At the same time, the Ni–C3 and Ni–C4 bond lengths are elongated and the biphenyl moiety that is forming is rotated slightly with respect to the coordination plane. The energy difference is quite large, with ΔE_{ZPE} = 14.7 and ΔG_{THF} = 20.9 kcal mol^{-1}. Then, the phenyl rings move closer to complete the C–C bond

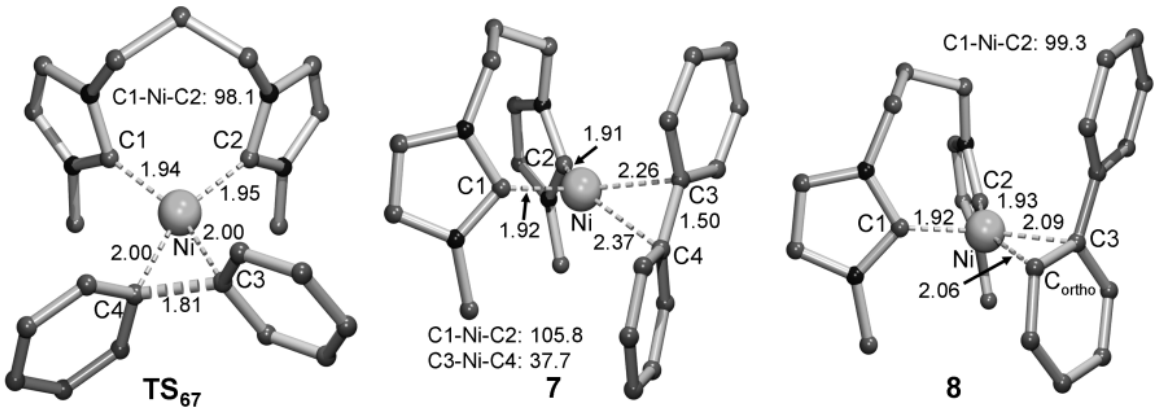

Figure 6.6. Geometries of the species involved in the reductive elimination, with calculated bond distances (Å) and angles (°). Hydrogen atoms are omitted for clarity.

formation, with the biphenyl moiety rotated more out of the coordination plane to give adduct **7**. As the structure approaches the Ni(0) species, the bisNHC bite angle widens to 105.8°, while the Ni–C1 and Ni–C2 bonds shorten slightly. Species **7** easily releases the biphenyl adduct to give the starting Ni(0) species **1**, which may participate in another catalytic cycle. The overall reductive elimination process is exothermic by 9.0 kcal mol^{-1}.

In addition to the η^2 adduct **7** complex **8** could be located with the nickel center bound to C3–C_{ortho}. In this case the biphenyl moiety is more tightly bound to the nickel center and the two phenyl rings are more rotated away from coplanarity. Species **8** has a free energy between that of **7** and the final Ni(0) species (ΔG_{THF} = –1.9 kcal mol^{-1}, relative to **6**). The fact that this stable complex could be identified may indicate that a ring walking mechanism is available for the product, as was the case before the oxidative addition step. No attempts were made to find transition states for this ring walk, as its barriers are probably low and the structures not important for the complete mechanism.

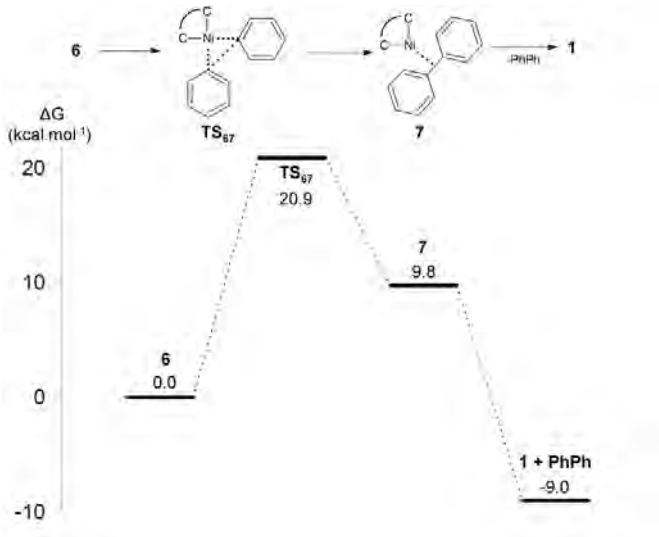

Scheme 6.5. Energy diagram for the reductive elimination step. Energy is given as Gibbs free energy in solution (THF, COSMO) relative to **6**.

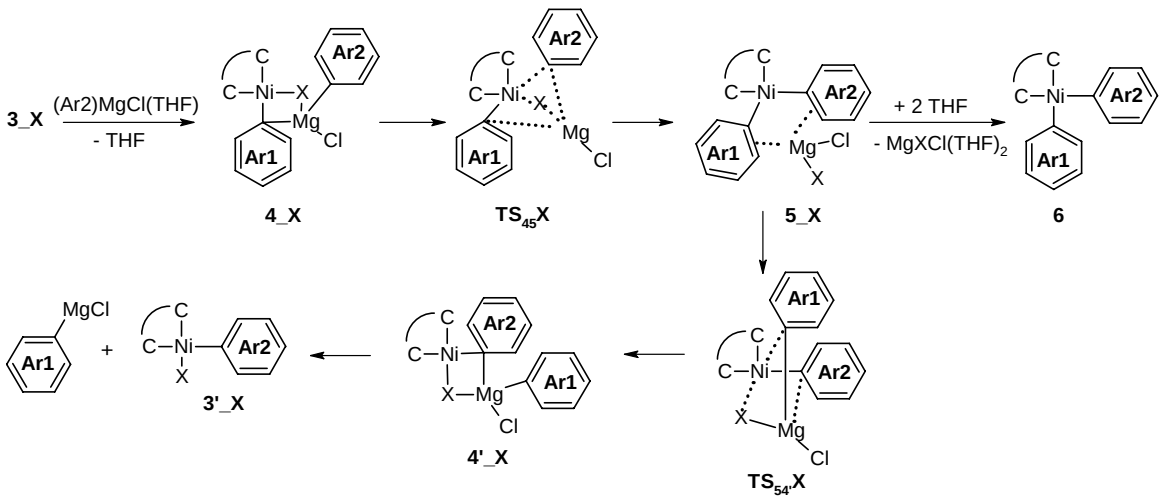

Scheme 6.6. Overview of the proposed aryl-exchange pathway. The two aryl rings are numbered according to their starting position (ring Ar1 originates from **3_X**, ring Ar2 originates from the Grignard reagent).

Aryl exchange

During the catalytic studies of the nickel-catalyzed Kumada coupling, a number of side products was observed.[10, 39] In particular, varying amounts of anisole, biphenyl and 4,4'-dimethoxybiphenyl could be detected (Scheme 6.2). Recently, it has been proposed that these side products are formed during the transmetalation step by exchange of the aromatic moieties on the nickel species and the Grignard reagent.[40] To incorporate this hypothesis in the present DFT study, it is proposed that the exchange takes place according to the route depicted in Scheme 6.6. The pathway calculated for the transmetalation sequence (**3_X** to **6**) if followed until intermediate **5_X**. From this intermediate the reaction may continue to give the desired diaryl complex **6**, or a reverse transmetalation may occur in which aryl ring Ar1 is replaced with the magnesium-bound halide. For this step a transition state **TS$_{54'}$X** is proposed which is the mirror image of transition state **TS$_{45}$X**, with a barrier of equal height. Dissociation of the newly formed phenylmagnesium chloride from intermediate **4'_X** effectively leads to an exchange of aryl rings between the nickel center and the magnesium ion.

In addition to the aryl exchange route depicted in Scheme 6.6, an alternative route starting from intermediate **4_X** was also considered. Whereas rotation about the Mg–C3 bond leads to transmetalation of the halide and the aryl ring, rotation about the Mg–X bond would lead to an exchange of aryl rings between the magnesium ion and the nickel center. Unfortunately, the transition state describing this movement could not be located.

Mechanistic considerations

In principle, the step in the catalytic cycle with the largest energy barrier to the transition state is rate determining. Taking into account the three steps of the

catalytic cycle and the energy barriers calculated for these steps, it is clear that all three steps have barriers of comparable magnitude of 20 – 25 kcal mol^{-1}. Therefore, the actual rate-determining step may be determined by subtle differences in the catalyst and the substrate. In the experimental catalytic studies (Chapter 4) it was observed that the rate of the reaction with 4-chloroanisole increases with the bulk of the side groups on the ligand, while with 4-bromoanisole the rate decreases with bulk.[10] Based on these observations, it was proposed that in the case of the aryl chloride the reductive elimination step must be rate determining, while with the aryl bromide substrate it must be either the transmetalation or the oxidative addition step. In agreement with these experimental observations, the barriers for the oxidative addition and the transmetalation of the bromo compounds were calculated to be slightly larger than the barriers for the oxidative addition and transmetalation of the chloro compounds.

The energy profiles for the complete catalytic cycle starting from chlorobenzene and bromobenzene are remarkably similar. The experimentally observed distinct reactivity of the two aryl halide substrates must therefore originate from rather small energy differences. The higher reactivity of aryl bromides compared to aryl chlorides may be explained by the initial coordination of the aryl halide to the nickel(0) species in the oxidative addition step, which was calculated to be slightly exothermic for aryl bromides and endothermic for aryl chlorides.

In Scheme 6.7 the steps are depicted that result from the aryl exchange pathway, under experimental conditions and which lead to the experimentally observed side products. The sequence starts with the exchange of the anisyl moiety on the nickel species (**A**) and the phenyl ring of the Grignard reagent. Subsequent reaction of nickel phenyl intermediate **B** with another Grignard reagent leads to biphenyl **iv**, while the anisyl Grignard reagent **C** eventually leads to the formation of

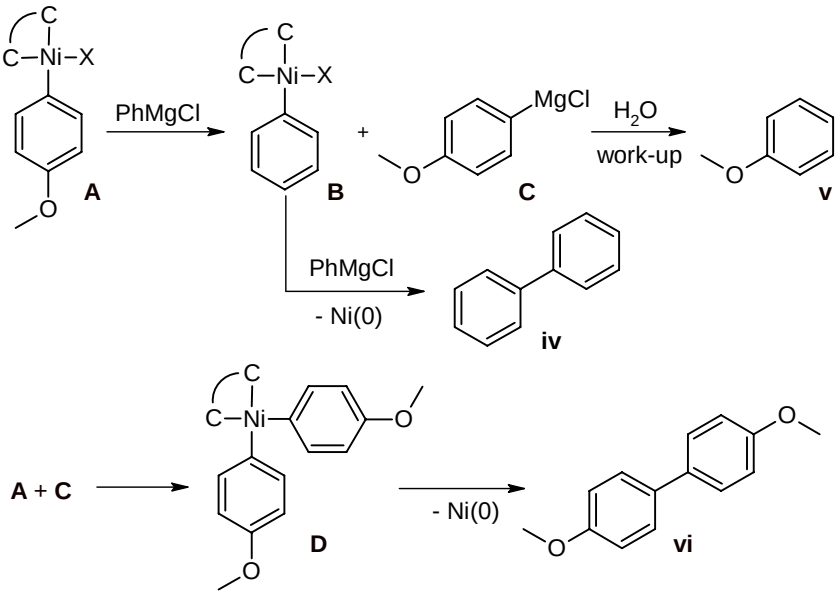

Scheme 6.7. Routes leading to the formation of side products **iv** - **vi**.

the 4,4′-dimethoxybiphenyl **vi** (by reacting with another species **A**) and anisole **v** (during work-up). According to this reaction scheme, the amount of biphenyl formed should be equal to the amount of anisole plus the amount of 4,4′-dimethoxybiphenyl. This correlates well with the experimental results.[10]

It was observed experimentally that a significantly larger amount of side products is formed during the coupling of 4-bromoanisole than with 4-chloroanisole. As both the transmetalation and the aryl exchange pathway have structure **5_X** as an intermediate, the differences observed in selectivity must originate here. Apparently, in the case of X = Br the rate of the reverse transmetalation is higher then with X = Cl. This is in agreement with the calculated energies of **5_X**, as for X = Br the barrier towards **TS$_{54'}$X** is lower than for X = Cl.

6.4 Conclusion

The complete pathway for the Kumada coupling of aryl halides with aryl Grignard reagents catalyzed by nickel complexes bearing a bisNHC ligand has been investigated theoretically at the BLYP/TZP level of theory with explicit solvent coordination and implicit COSMO solvent correction. The present calculations confirm the feasibility of the proposed route, consisting of oxidative addition, transmetalation and reductive elimination. The transmetalation step has been calculated with aryl Grignard reagents for the first time and is found to occur via a four-membered transition state with possible nickel-magnesium interaction. Moreover, the transmetalation sequence and the scrambling of aryl rings, leading to experimentally observed side products, have been proposed to evolve through a single intermediate species.

As the energy profiles calculated for the Kumada coupling of aryl chlorides and aryl bromides are quite similar, and as the rate-determining step could not be located unambiguously, it is difficult to correlate the calculations with experimental results. However, the fact that the barriers for the three steps in the catalytic cycle are calculated to be close in energy is in agreement with the experimentally observed change in rate-determining step when changing the substrate halide.

6.5 References

(1) Littke, A. F.; Fu, G. C. *Angew. Chem.-Int. Edit.* **2002**, *41*, 4176.
(2) Corbet, J. P.; Mignani, G. *Chem. Rev.* **2006**, *106*, 2651.
(3) Ahlquist, M.; Norrby, P. O. *Organometallics* **2007**, *26*, 550.
(4) Ariafard, A.; Lin, Z. Y. *Organometallics* **2006**, *25*, 4030.
(5) Fazaeli, R.; Ariafard, A.; Jamshidi, S.; Tabatabaie, E. S.; Pishro, K. A. *J. Organomet. Chem.* **2007**, *692*, 3984.
(6) Goossen, L. J.; Koley, D.; Hermann, H. L.; Thiel, W. *Organometallics* **2005**, *24*, 2398.
(7) Corriu, J. P.; Masse, J. P. *J. Chem. Soc.-Chem. Commun.* **1972**, 144.
(8) Tamao, K.; Sumitani, K.; Kumada, M. *J. Am. Chem. Soc.* **1972**, *94*, 4374.

(9) Tamao, K. *J. Organomet. Chem.* **2002**, *653*, 23.
(10) Berding, J.; Lutz, M.; Spek, A. L.; Bouwman, E. *Organometallics* **2009**, *28*, 1845.
(11) Yoshikai, N.; Matsuda, H.; Nakamura, E. *J. Am. Chem. Soc.* **2008**, *130*, 15258.
(12) Penka, E. F.; Schlapfer, C. W.; Atanasov, M.; Albrecht, M.; Daul, C. *J. Organomet. Chem.* **2007**, *692*, 5709.
(13) Radius, U.; Bickelhaupt, F. M. *Organometallics* **2008**, *27*, 3410.
(14) Green, J. C.; Herbert, B. J.; Lonsdale, R. *J. Organomet. Chem.* **2005**, *690*, 6054.
(15) ADF2006.01, *SCM, Theoretical Chemistry, Vrije Universiteit, Amsterdam, The Netherlands, http://www.scm.com*.
(16) Fonseca Guerra, C.; Snijders, J. G.; te Velde, G.; Baerends, E. J. *Theor. Chem. Acc.* **1998**, *99*, 391.
(17) Te Velde, G.; Bickelhaupt, F. M.; Baerends, E. J.; Guerra, C. F.; Van Gisbergen, S. J. A.; Snijders, J. G.; Ziegler, T. *J. Comput. Chem.* **2001**, *22*, 931.
(18) Becke, A. D. *Phys. Rev. A* **1988**, *38*, 3098.
(19) Lee, C. T.; Yang, W. T.; Parr, R. G. *Phys. Rev. B* **1988**, *37*, 785.
(20) Klamt, A. *J. Phys. Chem.* **1995**, *99*, 2224.
(21) Klamt, A.; Schuurmann, G. *J. Chem. Soc.-Perkin Trans. 2* **1993**, 799.
(22) Zhu, W. H.; Wu, G. S.; Jiang, Y. S. *Int. J. Quantum Chem.* **2002**, *86*, 347.
(23) Bohm, V. P. W.; Herrmann, W. A. *Angew. Chem.-Int. Edit.* **2000**, *39*, 4036.
(24) Scott, N. M.; Clavier, H.; Mahjoor, P.; Stevens, E. D.; Nolan, S. P. *Organometallics* **2008**, *27*, 3181.
(25) Smith, M. B.; Becker, W. E. *Tetrahedron* **1967**, *23*, 4215.
(26) Holm, T. *Acta Chem. Scand.* **1969**, *23*, 579.
(27) Ehlers, A. W.; van Klink, G. P. M.; van Eis, M. J.; Bickelhaupt, F.; Nederkoorn, P. H. J.; Lammertsma, K. *J. Mol. Model.* **2000**, *6*, 186.
(28) Tammiku-Taul, J.; Burk, P.; Tuulmets, A. *J. Phys. Chem. A* **2004**, *108*, 133.
(29) Without explicit solvent interaction: $\Delta E(ZPE) = -51.6$ kcal/mol, $\Delta G(THF) = -52.8$ kcal/mol for X = Cl, $\Delta E(ZPE) = -50.5$ kcal/mol, $\Delta G(THF) = -51.6$ kcal/mol for X = Br.
(30) Reinhold, M.; McGrady, J. E.; Perutz, R. N. *J. Am. Chem. Soc.* **2004**, *126*, 5268.
(31) Surawatanawong, P.; Fan, Y.; Hall, M. B. *J. Organomet. Chem.* **2008**, *693*, 1552.
(32) Arduengo, A. J.; Gamper, S. F.; Calabrese, J. C.; Davidson, F. *J. Am. Chem. Soc.* **1994**, *116*, 4391.
(33) Lin, B. L.; Liu, L.; Fu, Y.; Luo, S. W.; Chen, Q.; Guo, Q. X. *Organometallics* **2004**, *23*, 2114.
(34) Alvarez, R.; Faza, O. N.; de Lera, A. R.; Cardenas, D. J. *Adv. Synth. Catal.* **2007**, *349*, 887.
(35) Wendt, O. F. *Curr. Org. Chem.* **2007**, *11*, 1417.
(36) Please note that the structures calculated for the transmetalation step are mirrored, compared to those of the other steps. This does not affect the outcome of the energy calculations.
(37) Ananikov, V. P.; Musaev, D. G.; Morokuma, K. *Organometallics* **2005**, *24*, 715.
(38) Huang, Y. L.; Weng, C. M.; Hong, F. E. *Chem.-Eur. J.* **2008**, *14*, 4426.
(39) Wolf, J.; Labande, A.; Daran, J. C.; Poli, R. *J. Organomet. Chem.* **2006**, *691*, 433.
(40) Richardson, J. M.; Jones, C. W. *J. Mol. Catal. A-Chem.* **2009**, *297*, 125.